Bioresource Technology 461 (2026) 135473

Contents lists available at ScienceDirect

Bioresource Technology

journal homepage: www.elsevier.com/locate/biortech

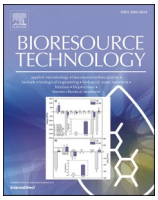

Oxygen-dependent redox control enables growth-decoupled biotransformations in *Cupriavidus necator*

Vivien Jesenofsky, Janek R. Weiler, Johannes Gescher, Miriam Edel *

Institute of Technical Microbiology, Hamburg University of Technology, 21073 Hamburg, Germany

HIGHLIGHTS

- Oxygen availability controls redox biotransformations in *Cupriavidus necator*.
- Anoxia enables 93% efficient acetoin-to-2,3-butanediol conversion.
- Oxygen rapidly reoxidizes 2,3-butanediol and suppresses its accumulation.
- Respiratory control enables glycerol-to-1,3-propanediol production.
- *Cupriavidus necator* remains viable under anoxia for prolonged biotransformations.

GRAPHICAL ABSTRACT

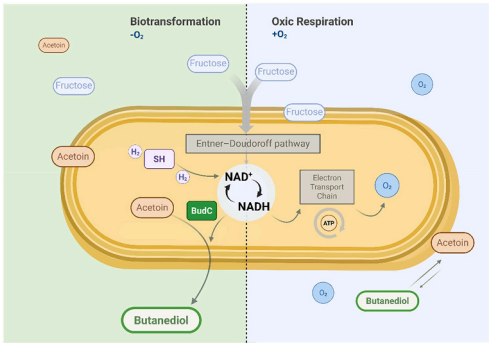

ABSTRACT

Genetic instability and environmental heterogeneity present persistent challenges to the stable microbial production of reduced, value-added chemicals. This work shows that limiting oxygen availability redirects electrons from respiration toward targeted reductive pathways in *Cupriavidus necator,* steering growth-decoupled biotransformations — exemplified by the conversion of acetoin to 2,3-butanediol and of glycerol to 1,3-propanediol. In cell suspension assays under a hydrogen-containing atmosphere, anoxic conditions stabilised near-stoichiometric acetoin-to-2,3-butanediol conversion (93% molar efficiency) despite minimal fructose consumption, indicating that the reductive pathway served as the primary sink for reducing equivalents. Under oxic conditions, rapid product re-oxidation lowered the final 2,3-butanediol titre to 2.6 mM. The same principle extended to 1,3-propanediol formation in a glycerol-kinase-deficient strain: anoxic incubation yielded 6.6 mM 1,3-propanediol, whereas aerobic conditions suppressed accumulation despite rapid substrate uptake. Viability assays showed that *Cupriavidus necator* retained above 84% viable cells under electron-acceptor exclusion for 144 h, declining to about 68% at 312 h and below 30% by 696 h, with cell aggregation from 48 h onward. This defined operational window, together with the lithoautotrophic capability of the organism, distinguishes the approach. By providing a metabolic configuration in which loss of production would be expected to be selectively disfavored, oxygen-controlled redox steering offers a route toward more robust reductive biotransformations. Oxygen availability thus acts as a single, tunable lever determining whether reducing equivalents flow into reduced products or into respiration.

1. Introduction

The production of high-value compounds via synthetic pathways in microorganisms is a persistent challenge because engineered systems are prone to genetic instability. During prolonged, high-density cultivation, spontaneous replication errors and strong selective pressures in large

* Corresponding author at: Institute of Technical Microbiology, Hamburg University of Technology, 21073 Hamburg, Germany.
E-mail address: miriam.edel@tuhh.de (M. Edel).

https://doi.org/10.1016/j.biortech.2026.135473
Received 21 April 2026; Received in revised form 19 July 2026; Accepted 20 July 2026
Available online 21 July 2026

populations can favor nonproducing “cheater variants” (Rugbjerg et al. 2018; Rugbjerg und Sommer 2019). Cells acquiring loss-of-function mutations in the synthetic pathway gain a significant fitness advantage by shedding metabolic burden, eventually outcompeting high-producing strains and causing process titers to decline (Rugbjerg et al. 2018; Rugbjerg und Sommer 2019). Beyond replication-dependent errors, genetic robustness is further compromised by growth-independent rearrangements, such as the activity of insertion sequences (IS elements), which can disrupt heterologous genes regardless of the culture's growth state (Vandecraen et al. 2017). While strategies like synthetic addiction and genome reduction aim to enforce genetic stability, they often impose heavy metabolic costs or impair environmental stress tolerance (Rugbjerg et al. 2018; Karcagi et al. 2016). Beyond genetic factors, environmental heterogeneity in bioreactors further exacerbates phenotypic diversification. Large-scale fermentations are characterized by spatiotemporal gradients in key process parameters, such as substrate and dissolved oxygen, due to imperfect mixing (Lara et al. 2006). As a result, individual cells experience rapidly fluctuating microenvironments, leading to heterogeneous metabolic states, growth rates, and stress responses within isogenic populations. These fluctuations can additionally promote the emergence of subpopulations with distinct physiological traits, including non-producing or low–producing phenotypes, thereby reducing overall process performance (Enfors et al. 2001; Neubauer und Junne 2010). Such scale-dependent heterogeneity remains a major challenge in industrial fermentation, as it is difficult to predict and control during scale-up.

Controlling the redox state of a culture through precise manipulation of oxygen availability provides a strategy to address both challenges: enforcing metabolic flux through a desired pathway, while potentially reducing the selective advantage of non-producing variants and reducing the impact of environmental heterogeneity on product yields (Rugbjerg et al. 2018). This study explores this strategy in *Cupriavidus necator* (*C. necator)*, a facultative chemolithoautotroph capable of producing a broad range of value–added chemicals through both native and engineered pathways, ranging from polyhydroxyalkanoates (PHAs) to 3-hydroxypropionic acid (3-HP), acetoin, 2,3–butanediol (2,3-BDO), and complex sesquiterpenes, such as α-humulene (Li et al. 2012; Weiler et al. 2024; Windhorst and Gescher 2019; Härrer et al. 2021; Becker et al. 2025). Its branched respiratory chain supports growth across a wide range of oxygen tensions, whereas anaerobic respiration is restricted to denitrification (Pohlmann et al. 2006). This respiratory plasticity renders it a particularly suitable host for redox-based process control.

This respiratory plasticity is harnessed here to steer two reductive biotransformations by modulating electron-acceptor availability. The first is the reduction of acetoin to 2,3-BDO, a reversible reaction catalyzed by a butanediol dehydrogenase; whereas 2,3-BDO yields typically suffer from re-oxidation in the presence of oxygen, an anoxic state enforces accumulation of the reduced product by eliminating the respiratory electron sink. The second, more complex case, is the conversion of glycerol to 1,3-propanediol (1,3-PDO): under anoxia, the intermediate 3-hydroxypropionaldehyde is no longer oxidized to 3-HP and routed into the tricarboxylic acid cycle via malonyl-CoA, but is instead reduced to the desired product. Both processes were conducted under a hydrogen-containing atmosphere with fructose as carbon source. *C. necator* metabolizes fructose exclusively via the Entner-Doudoroff (ED) pathway, due to its lack of a phosphofructokinase (Alagesan et al. 2018), yielding only one net ATP per hexose by substrate-level phosphorylation, so that respiratory ATP generation is critical for viability. Hydrogen can be co-oxidized by the hydrogenases of *C. necator*, the soluble enzyme reducing NAD^+ to NADH; under these lithoheterotrophic conditions it provides reducing equivalents but no additional ATP. As the medium contains no nitrate — the only anaerobic respiratory option in *C necator* H16 — no respiratory electron acceptor is available under the imposed anoxia, so the reductive biotransformations become the sole sink for the NADH generated from both fructose catabolism and hydrogen oxidation. This sustains metabolism while minimizing growth, a configuration expected to stabilize pathway flux and, by coupling catabolism to product formation, to disfavor non-producing variants.

2. Material & Methods

2.1. Chemicals

All chemicals were purchased from Carl Roth (Karlsruhe, Germany) or Merck (Darmstadt, Germany). Gas mixtures were supplied by Westfalen (Münster, Germany).

2.2. Strains and media

All strains and plasmids used in this study are listed in the supplementary material. For clarity, the key C. necator strains used throughout the results section are summarized in Table 1.

C. necator strains were cultivated at 30 °C in lysogeny broth (LB) or minimal medium (MM) as described by Sydow *et al.* (Sydow et al. 2017). All experiments for acetoin conversion and glycerol conversion to 1,3-PDO were conducted under heterotrophic conditions in minimal medium (MM), supplemented with 20 mM fructose and either 20 mM acetoin or 40 mM glycerol. Depending on the experimental setup, the headspace composition was adjusted to investigate the effect of oxygen availability. For oxygen-onset conditions, the headspace contained 80% H_2, 5% CO_2, and 15% O_2. For oxygen-offset conditions, O_2 was omitted and replaced with CO_2 (80% H_2, 20% CO_2).

Escherichia coli WM3064 was cultivated in LB medium at 37 °C supplemented with 0.3 mM diaminopimelic acid (DAP). When required, kanamycin was added at 250 μg mL^{-1} for *C. necator* and 50 μg mL^{-1} for *E. coli* (stock solution: 50 mg mL^{-1} in water). Solid media contained 2% (w/v) agar. All media were autoclaved at 121 °C for 20 min. Antibiotics, vitamin solutions, and fructose were sterilized by filtration through 0.22 μm membranes.

Explosive gas mixtures were handled in dedicated fume hoods equipped with continuous gas exhaust and explosion protection systems. Gas was transferred into sealed Schott bottles fitted with appropriate plugs and mounted upside down to prevent leakage.

2.3. Genetic construction

Diagnostic PCR was performed using MangoMix (Bioline, Luckenwalde, Germany). Preparative PCR was carried out using HIFI Polymerase (Nippon Genetics Europe, Düren, Germany) or PCRBIO Ultra Polymerase (PCR Biosystems Ltd., London, UK). PCR products were analyzed by agarose gel electrophoresis and purified using the Wizard® SV Gel and PCR Clean-Up System (Promega, Mannheim, Germany). Plasmids were isolated using the Wizard® Plus SV Minipreps DNA Purification System (Promega). Restriction enzymes were obtained from New England Biolabs (Frankfurt, Germany), and oligonucleotides were synthesized by Merck (Darmstadt, Germany). All constructs were

Table 1
Overview of the engineered **C. necator** strains used in this study. The strains shown were used for the oxygen-dependent biotransformation of acetoin to 2,3–BDO and glycerol to 1,3-PDO.

Strain	Genotype	Role in study
JG2058	Δ*acoABC* Δ*phaC*1 Δ*phaC*2 Δ*HoxKGM* + pBBR1-*budC*	Oxygen-dependent acetoin reduction
JG2052	Δ*phaC1/C*2 Δ*glpK*1 Δ*glpK*2 Δ*HoxKGM* + pBBR1-*dhaB2TB1*	Oxygen-dependent 1,3–PDO production
JG2053	Δ*phaC1/C*2 Δ*glpK*1 Δ*glpK*2 Δ*HoxKGM* + pBBR1MCS-2	Empty-vector control

verified by Sanger sequencing (Eurofins Genomics, Ebersberg, Germany) and sequence alignment using Benchling (Biology Software (2025/2026) San Francisco, USA).

2.4. Plasmid Construction for Overexpression

2.4.1. Butanediol Production Plasmid

The expression plasmid was constructed based on the system described by Weiler et al. (2024), utilizing the native PHB promoter system and the *budC* Gene from *Enterobacter cloacae* but not the *alsSD* gene cluster. The parental plasmid (Weiler et al., 2024) was modified by inverse PCR. PCR products were treated with T4 Polynucleotide Kinase (NEB, Frankfurt, Germany) for 30 min at 37 °C to phosphorylate 5′-ends, followed by heat inactivation at 65 °C for 20 min. Self-ligation was performed using T4 DNA Ligase (Thermo Fisher Scientific, Waltham, USA) and heat inactivated at 70 °C for 5 min prior to electrotransformation into *E. coli* WM3064. The plasmid was subsequently conjugated into *C. necator*.

2.4.2. Propanediol Production Plasmid

The plasmid for 1,3-PDO production was synthesized by GeneArt (Thermo Fisher Scientific, Waltham, USA) based on a native gene cluster from *Clostridium butyricum*, which was codon-optimized for *C. necator*. The gene order within the operon was rearranged to *dhaB2–dhaT–dhaB1*, placing the activating factor (DhaB2) upstream of the propanediol dehydrogenase (DhaT) and the glycerol dehydratase (DhaB1). Individual genes were separated by ribosome binding sites (Shine–Dalgarno sequences) and spacer regions to facilitate balanced expression. The expression cassette was cloned into a pBBR1-based vector under control of the native PHB promoter of *C. necator*. The synthesized construct was delivered as a plasmid and subsequently digested with *Bsr*GI-HF and *Xho*I (New England Biolabs, Frankfurt, Germany). In parallel, the pBBR1 backbone containing the PHB promoter was digested with the same restriction enzymes. The insert and backbone were ligated using T4 DNA Ligase (Thermo Fisher Scientific, Waltham, USA) according to the manufacturer's instructions. The resulting plasmid was transformed into *E. coli* WM3064 and subsequently transferred into *C. necator* via conjugation. Further details on plasmid design and sequence composition are provided in the supplementary material.

2.5. Construction of Deletion Plasmids

Gene deletion constructs were generated by gene synthesis of 500 bp homologous regions up- and downstream of the target gene (ΔHoxKGM on megaplasmid: Δ90–4808; Δglycerol kinase on chromosome 1: 2718410–2719994; Δglycerol kinase on chromosome 2: 1354806–1356329; see supplementary material. Synthesized fragments contained 30 bp overlaps for a subsequent Gibson Assembly and were cloned into *Sal*I-HF/*Bam*HI-HF–linearized pMQ150, a suicide vector used for two-step allelic exchange in *C. necator* (Gibson et al. 2009). The Gibson mixture was dialyzed and transformed into *E. coli* WM3064 by electrophoresis. The conjugation was performed as described previously by Windhorst *et al.* (Windhorst and Gescher 2019). Single–crossover integrants were selected on kanamycin (250 μg mL^{-1}), followed by *sacB*-mediated counterselection on sucrose-containing medium to promote a second homologous recombination event. Putative deletion mutants were screened by colony PCR and verified by Sanger sequencing. Primers, restriction enzymes, and plasmids used in this study are listed in the supplementary material.

2.6. Growth experiment

Heterotrophic growth experiments of *C. necator* were performed under oxic conditions in shake flasks at 30 °C and 180 rpm until stationary phase was reached. Pre-cultures were grown overnight in LB medium, followed by two successive cultivations in minimal medium (MM) to minimize adaptation lag. Main cultures (25 mL working volume) were inoculated to an initial target OD_{600} of 0.08 in MM supplemented with 20 mM fructose and 20 mM acetoin. All experiments were performed as quadruplicates. Optical density at 600 nm (OD_{600}) was monitored at 12 time points over 76 h. For substrate analysis, 0.5 mL samples were withdrawn and analyzed for fructose and acetoin concentrations by high-performance liquid chromatography (HPLC).

2.7. Cell suspension assays

Cells were pre-cultivated overnight in LB medium for three successive cycles each inoculated at 1% (v/v) into increasing culture volumes.

For heterotrophic cell suspension experiments, cultures were harvested and adjusted to a targeted OD_{600} of 4 in 25 mL MM in sterile, gastight 1-L glass bottles sealed with rubber septa and incubated at 30 °C and 180 rpm. All experiments were conducted in triplicates.

Prior to gas application, bottles were degassed by alternating 2-min cycles of vacuum and N_2 flushing (1 bar) for 40 min. Subsequently, vacuum was applied for 20 min before introducing the respective cultivation gas mixture. The headspace composition was measured immediately after gassing. Liquid samples (0.5 mL) were aseptically withdrawn using sterile syringes equipped with cannulas for determination of OD_{600} and analysis of fructose, acetoin, 2,3-BDO, glycerol and 1,3-PDO concentrations by HPLC. For gas analysis, 30 mL headspace samples were collected through the septa using gas-tight syringes and immediately analyzed by micro gas chromatography (micro-GC). Pressure changes resulting from cultivation or sampling were compensated by re-adjusting the headspace to 1 bar using N_2.

2.8. Substrate and product analysis

2.8.1. High-performance liquid chromatography (HPLC)

Metabolite concentrations were quantified using a Thermo Scientific™ UltiMate™ 3000 UHPLC system (Thermo Fisher Scientific, Waltham, USA) equipped with a refractive index detector (RefractoMax 521, Thermo Fisher Scientific).

Samples (200 μL) were filtered through 0.2 μm PTFE membrane filters (VWR, Darmstadt, Germany) and mixed with 20 μL of 0.05 M H_2SO_4 in 96-well plates prior to analysis. Separation was performed on a Hi-Plex H column (7.7 × 300 mm, 8 μm; Agilent Technologies, Waldbronn, Germany) at 60 °C using 5 mM H_2SO_4 in ddH_2O as the mobile phase at a flow rate of 0.5 mL min^{-1}. Data acquisition and analysis was conducted using Chromeleon 7.2 SR4 software (Thermo Fisher Scientific).

2.8.2. Micro Gas Chromatography (Micro-GC)

Headspace gas composition (H_2, O_2, N_2, and CO_2) was analyzed using a 490 Micro GC system (Agilent Technologies, Waldbronn, Germany). Data acquisition and processing were performed with Agilent OpenLAB CDS (EZChrom Edition). The method parameters included a stabilization time of 5 s, a sampling time of 30 s, and an injector time of 50 ms. The transfer line between sample inlet and injector was maintained at 110 °C. Permanent gases (H_2, O_2, and N_2) were separated on a 10 m MS5A column using argon as carrier gas at 70 °C and 150 kPa. CO_2 was separated on a 10 m PPQ column using helium as carrier gas at 45 °C and 150 kPa.

2.9. Microscopy

For each replicate, three images per sampling point were acquired using a Leica DM5500B microscope (Leica Microsystems, Wetzlar, Germany) equipped with L5 and Y3 fluorescence filters. All images were acquired at 318 ms exposure with 33% lamp intensity to reduce phototoxicity, with identical parameters across all experiments.

2.9.1. Live / Dead-Staining

Cell viability was assessed by SYTO9/propidium iodide (PI) staining (Invitrogen, Thermo Fisher Scientific, Oregon, USA). Staining solution was prepared by mixing 5 mM SYTO9 and 20 mM PI stock solutions 1:1, then diluting the mixture 1:500 in Sydow minimal salt solution under light-protected conditions; it was used within 48 h (max. one freeze–thaw cycle).

For cell immobilization, 0.2% (w/v) low-melt agarose (LMA) was boiled, cooled to 37° C, and mixed 1:1 (v/v) with cell suspension (25 µL each). 2 µL of the mixture were transferred per well onto 8-well microscopy slides (6 mm, Thermo Scientific, Portsmouth, UK), with one well per condition and replicate. 15 µL of staining solution were added per well, incubated 10 min in the dark, excess solution removed, and 5 µL Sydow minimal salt solution added before coverslipping. Slides were stored at 4°C and imaged within 3 h of staining.

2.9.2. Quantification

Cells were quantified using a custom FIJI macro (v1.54p) based on the Find Maxima function (prominence: 10,000; output: count). Since SYTO9 stains all cells and PI only those with damaged membranes, a second macro identified overlapping signals in both channels using the Overlap Extractor tool (BioVoxxel3DBox for ImageJ; same prominence; volume range 0–100; all other options false); overlapping signals were counted as dead cells and subtracted from the SYTO9 count to omit double-counting.

Samples with fewer than 100 total signals were excluded. For each replicate, the median viability across the three images was calculated; images deviating > 20% from the median were excluded as optical artifacts (14 of 250 images total). Signals from the remaining images per sample were pooled and the live-to-dead ratio calculated. To account for methodological variation across sampling points, the highest live-cell count per time point was set as 100% survival, and all other ratios at that time point were normalized accordingly. Samples from both experimental conditions (±oxygen) were always collected simultaneously to enable this normalization. Finally, the mean and standard deviation across replicates were calculated for each sampling time.

2.10. Determination of intracellular ATP levels

Triplicate cell suspension assays were performed under anoxic conditions as described using a target OD_{600} of 4. Cell suspensions were supplemented with either 20 mM acetoin and 20 mM fructose or 20 mM 2,3-BDO and 20 mM fructose. At the indicated time points, samples were collected for ATP determination, OD_{600}, pH measurements and HPLC analysis as described above. Intracellular ATP levels were determined using the BacTiter-Glo™ Microbial Cell Viability Assay (Promega, Madison, WI, USA). Samples were diluted 1:10 in the respective assay medium. Luminescence was measured in white 96-well microplates (Greiner Bio-One, Frickenhausen, Germany) using a Tecan Infinite® 200 PRO microplate reader (Tecan, Männedorf, Switzerland). ATP levels were normalized to the corresponding OD_{600} values and expressed relative to the initial measurement ($t_0 = 100\%$).

3. Results

3.1. Growth and Biotransformation Dynamics During Oxic Cultivation with Fructose and Acetoin

To investigate oxygen-dependent acetoin reduction, strain JG2058 (Δ*acoABC* Δ*phaC*1 Δ*phaC*2 Δ*HoxKGM* carrying pBBR1-*budC*) was cultivated on fructose supplemented with acetoin under oxic conditions. Fructose was rapidly consumed, with its concentration decreasing from 20.2 mM to 1.7 mM within 17 h (Fig. 1). The highest fructose consumption rate occurred between 8 and 14 h, reaching approximately 2 $mM{\cdot}h^{-1}$, followed by a decline indicative of substrate limitation. The specific growth rate (µ) during exponential growth was 0.3 ± 0.1 h^{-1}, corresponding to a doubling time of 2.8 h.

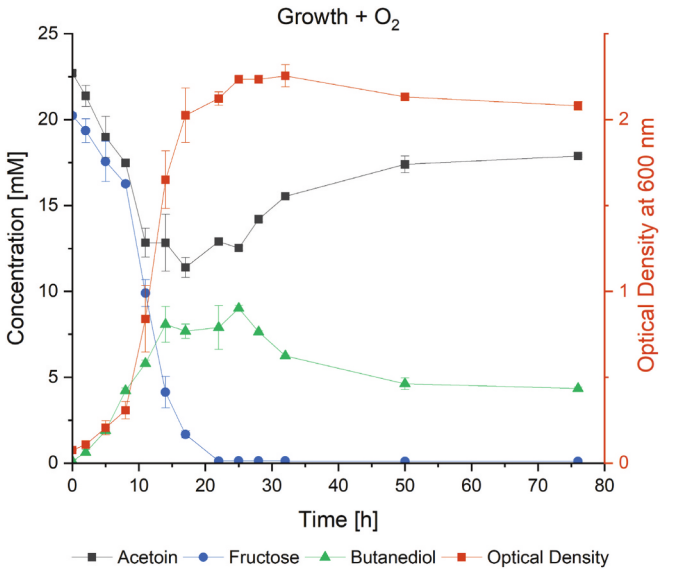

Fig. 1. Growth-coupled acetoin conversion under oxic conditions. Fructose is rapidly consumed, supporting biomass formation and transient 2,3-BDO production. As growth proceeds, 2,3-BDO concentrations decline while acetoin accumulates, indicating oxygen-dependent re-oxidation.

Concurrently, acetoin was reduced to 2,3-BDO during the early growth phase. Between 0 and 11 h, acetoin concentration decreased from 22 mM to 12.8 mM at an average rate of 0.9 $mM{\cdot}h^{-1}$, while 2,3–BDO accumulation reached 8 mM by 14 h with a mean conversion rate of 0.7 $mM{\cdot}h^{-1}$ (between 5 and 14 h) (Fig. 1). Thereafter, a reversal of the biotransformation was observed. Between 14 and 50 h, 2,3-BDO concentrations decreased from 8 mM to 4.6 mM, while acetoin levels rose from 12.8 mM back to 17.4 mM. Thus, depletion of the growth substrate fructose and the presence of oxygen seemed to be the trigger for re-oxidation of butanediol to acetoin and NADH and the subsequent use of NADH to drive oxidative phosphorylation.

3.2. Cell suspension assays under oxic and anoxic conditions reveal distinct fructose utilization and acetoin conversion

To determine whether oxygen depletion could stabilize production towards butanediol, cell suspension assays were conducted with an initial target OD_{600} of 4 to assess biotransformation under both anoxic and oxic conditions. Under anoxic conditions, the OD_{600} decreased slightly from 4.4 to 3.6 over the 72-hour incubation (Fig. 2b). Fructose consumption proceeded slowly, with 4.8 mM of substrate utilized within the first 24 h, corresponding to a mean consumption rate of 0.2 $mM{\cdot}h^{-1}$. Despite limited fructose assimilation, efficient conversion of acetoin to 2,3-BDO was observed. Acetoin fully converted within 24 h, exhibiting a maximum conversion rate of 2.1 $mM{\cdot}h^{-1}$ between 3 and 9 h, and a mean rate of 0.8 $mM{\cdot}h^{-1}$ over 24 h. Concurrently, 2,3-BDO accumulated with a mean production rate of 0.7 $mM{\cdot}h^{-1}$ and a peak rate of 1.9 $mM{\cdot}h^{-1}$ between 3 and 9 h. Over 24 h, 20.1 mM acetoin was consumed, and 18.8 ± 0.5 mM 2,3-BDO was formed, demonstrating a near-equimolar conversion. About 2 mM of acetate were detected after 24 h under anoxic conditions as additional end product. Measurements, extended to 72 h, confirmed that these levels remained stable, with 0.8 ± 0.01 mM acetoin and 18.9 mM 2,3-BDO detected, while fructose consumption plateaued at 4.8 mM. In contrast, under oxic conditions, fructose was rapidly depleted, with only 1.4 mM remaining from an initial 21.7 mM after 9 h, corresponding to a mean consumption rate of 2.3 $mM{\cdot}h^{-1}$ (Fig. 2a). Acetoin conversion to 2,3-BDO occurred primarily within the first 9 h, at a mean rate of 2.2 $mM{\cdot}h^{-1}$. After this period, a back-conversion of 2,3-BDO to acetoin was observed, with a conversion rate of 0.9 $mM{\cdot}h^{-1}$

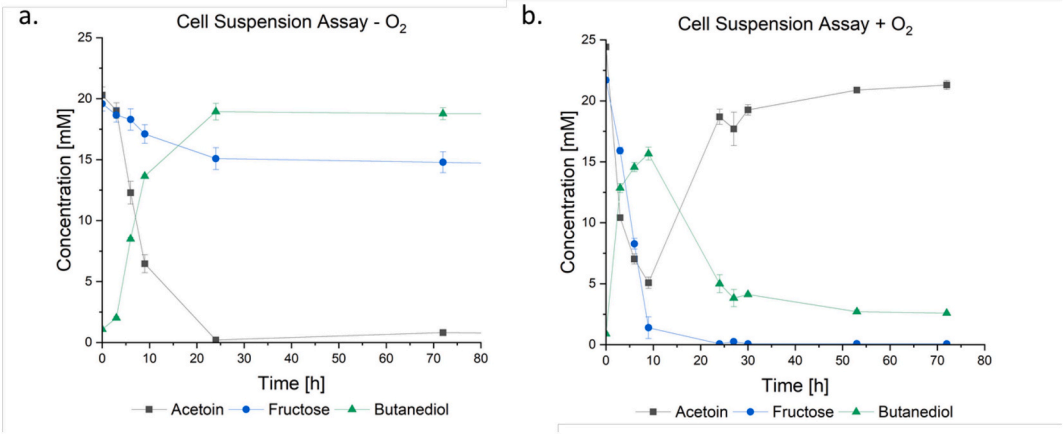

Fig. 2. Oxygen-dependent biotransformation of acetoin to 2,3-butanediol in cell suspension assays. (a) Under − O_2, acetoin is efficiently reduced to 2,3–BDO with minimal re-oxidation and reduced fructose consumption. (b) Under + O_2, fructose is rapidly consumed and 2,3-BDO formation is transient, followed by re-oxidation to acetoin.

between 9 and 24 h. Starting from an initial acetoin concentration of 24.4 mM, 5.1 mM remained at 9 h, rising again to 18.7 mM by 24 h. Correspondingly, 2,3-BDO accumulated to a maximum concentration of 15.7 mM at 9 h, followed by a decline to 5 mM at 24 h. The production rate of 2,3–BDO was 1.6 mM·h^{-1} during the first 9 h, decreasing to a back-conversion rate of 0.7 mM·h^{-1} between 9 and 24 h. Monitoring at

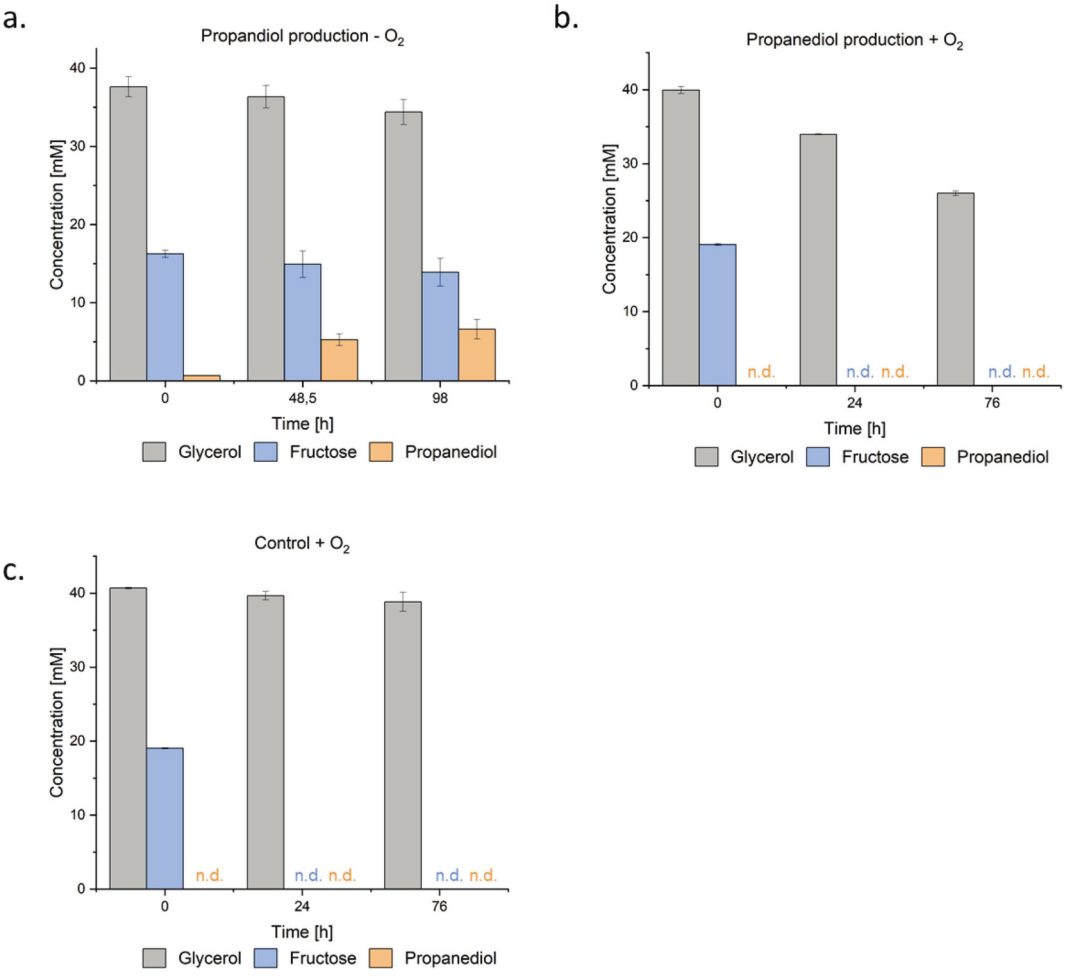

Fig. 3. Oxygen-dependent production of 1,3-propanediol from glycerol in cell suspension assays. (a) Recombinant strain JG2052 expressing the heterologous *dhaB2–dhaT–dhaB1* operon under anoxic conditions (−O_2). Substrate consumption proceeded gradually, with decreases in glycerol and fructose accompanied by continuous accumulation of 1,3-PDO. Samples were collected after 0, 48.5, and 98h. (b) The same strain under oxic conditions (+O_2). Fructose was rapidly depleted and glycerol was partially consumed; however, no detectable 1,3-propanediol was formed. Samples were collected after 0, 24, and 76h. (c) Control strain carrying the empty plasmid under oxic conditions (+O_2). Fructose was consumed whereas glycerol remained largely unchanged, and no detectable 1,3-PDO was observed. Samples were collected after 0, 24, and 76h.

72 h revealed that the back reaction continued at a slower rate, with acetoin increasing to 21.3 ± 0.4 mM and 2,3–BDO decreasing further to 2.6 ± 0.04 mM; fructose was nearly depleted, with 0.1 mM remaining at 72 h. Comparison of the final product titers demonstrated a significant difference between anoxic and oxic conditions, with 18.9 ± 0.6 mM and 2.6 ± 0.04 mM 2,3-BDO detected after 72 h, respectively (Welch's two-sided *t*-test, $p < 0.001$). Likewise, residual acetoin concentrations differed significantly between conditions (0.2 ± 0.07 mM vs. 21.3 ± 0.4 mM; Welch's two-sided *t*-test, $p < 0.001$). Thus, oxygen limitation significantly stabilized 2,3-BDO accumulation, consistent with the prevention of NADH reoxidation via aerobic respiration.

3.3. Application of respiratory control to 1,3-Propanediol production from Glycerol: An Outlook

To extend the concept of respiratory modulation for enhanced biotransformation stability, this strategy was applied to the production of 1,3-PDO from glycerol. For this purpose, strain JG2052 (Δ*phaC1/C2* Δ*glpK1* Δ*glpK2* Δ*HoxKGM* carrying the heterologous *dhaB2–dhaT–dhaB1* operon) was constructed based on a glycerol kinase-deficient *C. necator* background to prevent catabolic glycerol assimilation via glycerol-3-phosphate. To verify that the introduced mutations abolished catabolic glycerol utilization, a cell suspension assay was performed at an OD_{600} of 4. Glycerol and fructose consumption were monitored under oxic conditions (Fig. 3). Fructose was rapidly depleted, and within 24 h approximately 19 mM were consumed. In contrast, no significant glycerol utilization was observed, and after 76 h 38.8 (±1.3) mM glycerol remained in the medium. Consistently, no detectable end products were formed.

In this mutant, a glycerol dehydratase, its activating factor and a propanediol dehydrogenase were heterologously expressed to redirect glycerol flux toward 1,3–PDO via 3-hydroxypropionaldehyd as an intermediate. As previously demonstrated by Salinas et al. (2022), 3-hydroxypropionaldehyd can alternatively be oxidized to malonic semialdehyde and further metabolized to acetyl-CoA, feeding the citric acid cycle and enabling complete substrate mineralization. It was therefore hypothesized that, analogous to the findings with the acetoin system, blocking respiratory electron disposal would suppress this oxidative bypass and instead channel flux toward reductive 1,3-PDO formation.

To test this, cell suspension assays were performed under oxic and anoxic conditions starting from a target OD_{600} of 4. Under oxic conditions (Fig. 3b), glycerol uptake was substantial—13.9 mM consumed from an initial 40 mM over 76 h—and fructose was fully depleted within 24 h (19.1 mM consumed). Crucially, however, no detectable 1,3-PDO accumulated under these conditions. This decoupling of glycerol consumption from product formation confirms that the heterologously introduced pathway is metabolically active and capable of processing glycerol, but that under oxic conditions the intermediate 3-hydroxypropionaldehyd is preferentially oxidized and mineralized to carbon dioxide via the citric acid cycle rather than reduced to 1,3–propanediol. A potential metabolic route was described previously (see below).

Switching to anoxic conditions (Fig. 3a) resolved this uncoupling and directed flux toward the desired product. Substrate consumption was slower—glycerol decreased by 3.2 mM from an initial 37.6 mM and fructose by 2.4 mM from 16.3 mM over 98 h yet 6.6 mM 1,3-PDO accumulated during this period. On a carbon basis the two substrates were co-utilised rather than glycerol serving as the sole carbon source: the 2.4 mM fructose consumed corresponds to approximately 14 mM carbon, exceeding the approximately 10 mM carbon of the 3.2 mM glycerol consumed. The substrates fulfil distinct roles — glycerol is channelled to 1,3-PDO and provides the terminal electron sink, whereas fructose supplies carbon, substrate-level ATP, and reducing equivalents. These findings support that, under oxygen deprivation, the reductive conversion of 3-hydroxypropionaldehyd to 1,3-PDO becomes the dominant electron sink, enabling effective redox balancing and productive biotransformation despite minimal growth.

These observations highlight the potential of oxygen limitation as a lever to promote electron-sink-driven formation of reduced metabolites such as 1,3-PDO in *C. necator*. The parallels with the acetoin-to-2,3-BDO system suggest that dynamically controlling respiratory conditions could improve flux control and, potentially, evolutionary stability in biotechnologically relevant reductions.

3.4. Cell survival and viability under oxic and anoxic conditions

A switch to process conditions without terminal electron acceptor will exclude oxidative phosphorylation as ATP production route. To assess the long-term survival and hence ability to conduct the tested biotransformation of *C. necator* under different respiratory conditions, cell suspension assays were performed with an initial target OD_{600} of 3, supplemented with 20 mM fructose and 20 mM acetoin. Cultures were incubated either in the presence or absence of oxygen, and cell viability was monitored over an extended period of up to 744 h by measuring OD_{600} and performing live / dead–staining.

Under oxic conditions, the OD_{600} increased from 2.8 at the start of the experiment to a maximum of 4.4 within 48 h, indicating active growth (Fig. 4). Subsequently, the OD_{600} gradually declined to 3.38 at 312 h and stabilized around 3.3–3.4 for the remaining duration of the experiment. Live / dead-staining revealed that cell viability remained high throughout the incubation period, with live cell percentages persisting near or above 88% at all time points measured (Fig. 4a). Specifically, the fraction of live cells was 88.4% at time zero, peaked at 96.8% at 360 h, and maintained above 89% even at 744 h, demonstrating sustained viability under oxic conditions.

In contrast, under anoxic conditions, the OD_{600} remained relatively stable, with a slight increase from 2.7 to 2.8 during the first 48 h followed by a gradual decrease to 2.5 at 408 h and further down to 1.9 at 744 h (Fig. 4b). Despite the limited growth, cell viability was initially comparable to oxic conditions, with 90.3% live cells at time zero and remaining above 84% up to 144 h. However, a progressive decline in viability was observed starting after 192 h, dropping to 68% at 312 h and falling below 30% by 696 h (Fig. 4b). At the experiment's conclusion (744 h), approximately 26.2% of cells remained alive under oxygen-limited conditions.

Microscopic analysis revealed a distinct physiological response of *C. necator* to the absence of oxygen. After 48 h of incubation under anoxic conditions, a pronounced formation of cell aggregates was observed, which was not present under oxic conditions (Fig. 5). Representative microscopic images comparing samples at 0, 24, and 48 h with and without oxygen illustrate this phenomenon. Over the course of the experiment, aggregation intensified further in the anoxic samples, as documented in the supplementary material.

These observations indicate that while oxygen availability supports increased biomass formation and maintains high cell viability over extended periods, *C. necator* can survive for several weeks even in the absence of oxygen, albeit with reduced viability over time.

3.5. ATP maintenance during anoxic acetoin reduction

To assess whether acetoin reduction provides a physiological advantage under anoxic conditions, cell suspension assays were performed with the acetoin-producing strain in the presence of fructose and supplemented with either acetoin or 2,3-BDO. Relative intracellular ATP levels were determined over 24 h.

In acetoin-supplemented cultures, acetoin was continuously converted to 2,3–BDO, while relative ATP levels remained stable throughout the experiment, reaching 105.5 ± 29.9% and 113.2 ± 5.9% of the initial value after 9 h and 24 h, respectively (Fig. 6a). In contrast, cultures supplemented with 2,3-BDO showed only minor changes in extracellular metabolite concentrations, whereas ATP levels continuously declined to 71.8 ± 5.9% after 9 h and 62.7 ± 5.1% after 24 h (Fig. 6b). After 24 h, ATP levels were significantly higher in acetoin-

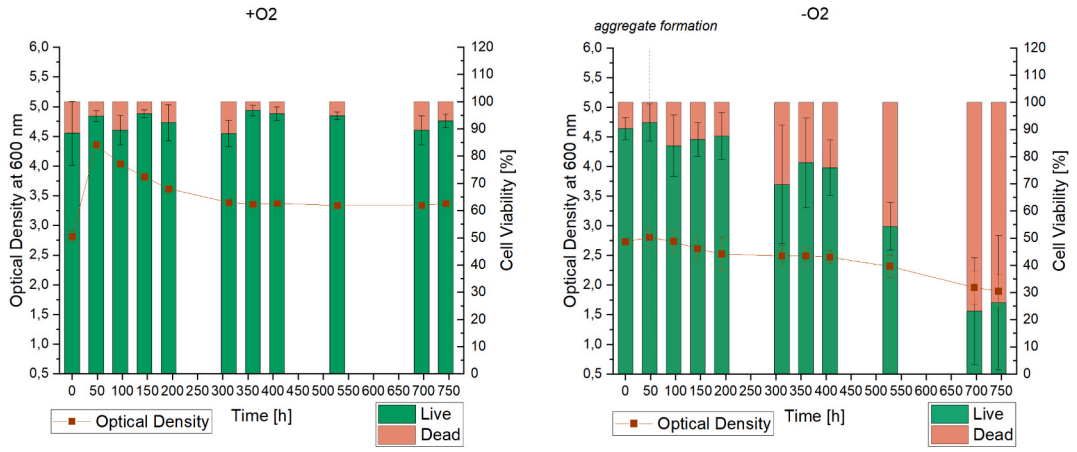

Fig. 4. Live / dead-stain assay of cells with and without oxygen. (a) Under + O_2, cell viability remained above 85% throughout the experiment. Rapid fructose consumption during the first 48 h was accompanied by biomass accumulation, which remained stable thereafter. (b) Under −O_2, cell viability declined over a time period of 750 h down to 26% while OD_{600} declined from 2.6 to 1.9.

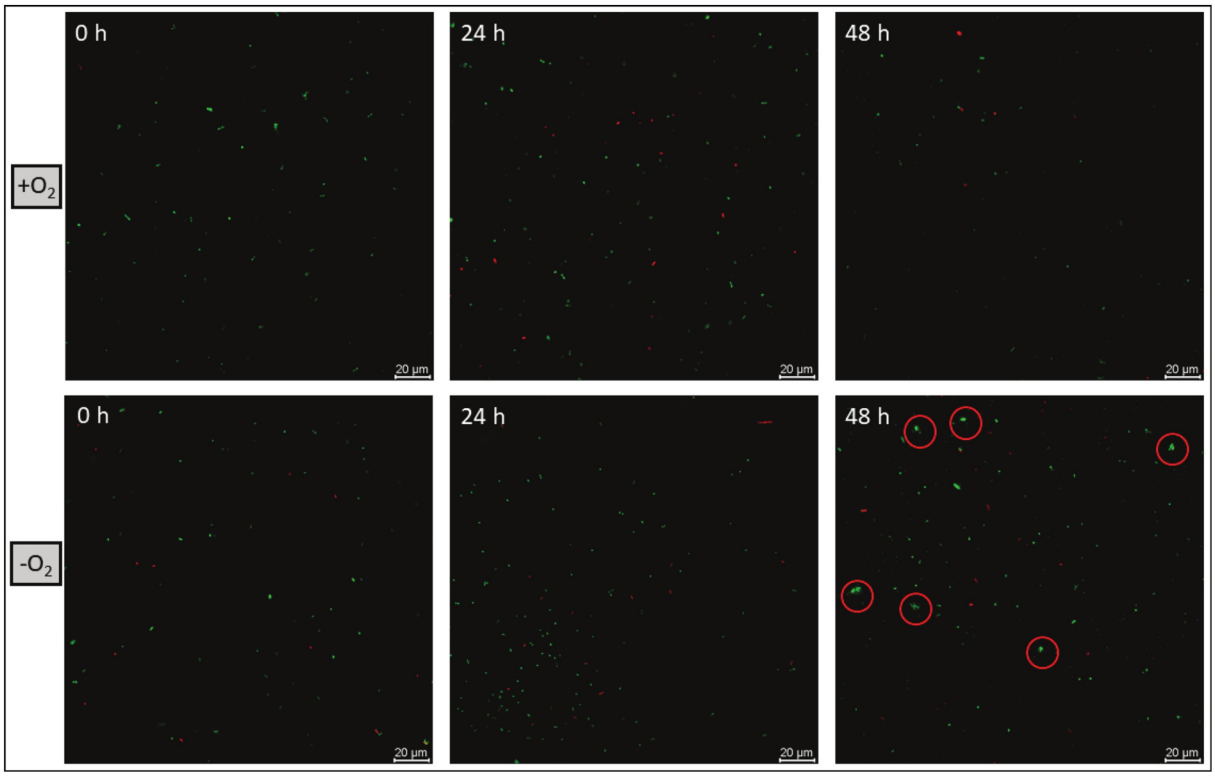

Fig. 5. Oxygen-dependent physiological response of *C. necator* to the absence of oxygen. Microscopic images at 0, 24 and 48 h of the live / dead-stain experiment showing a reaction of the cells to anoxic conditions. After 48 h under anoxic conditions, cells exhibited pronounced aggregate formation compared to oxic controls. Aggregate formation became increasingly pronounced over time (see supplementary material) and eventually diminished as cell viability declined, resulting in disintegration of the aggregates.

supplemented cultures than in cultures supplied with 2,3-BDO (Welch's two-sided *t*-test, $p < 0.001$). These findings indicate that acetoin reduction is associated with sustained ATP levels under anoxic conditions and supports the concept of coupling product formation to cellular fitness.

4. Discussion

4.1. Metabolic Insights from oxic growth of C. Necator

The oxic growth of *C. necator* on fructose and acetoin reveals important aspects of its metabolic priorities and redox balancing strategies during biotransformations. While oxygen serves as the preferred terminal electron acceptor—maximizing ATP generation through oxidative phosphorylation—the reduction of acetoin to 2,3–BDO remains an actively employed auxiliary pathway and significant NADH sink to maintain intracellular redox homeostasis.

In *C. necator*, fructose metabolism proceeds exclusively via the ED-pathway, yielding only one ATP per hexose molecule and producing one NADH and one NADPH molecule per substrate-level phosphorylation event—equivalent to 4 electrons (Rugbjerg et al. 2018). Complete oxidation of fructose to CO_2 via pyruvate dehydrogenase and the TCA

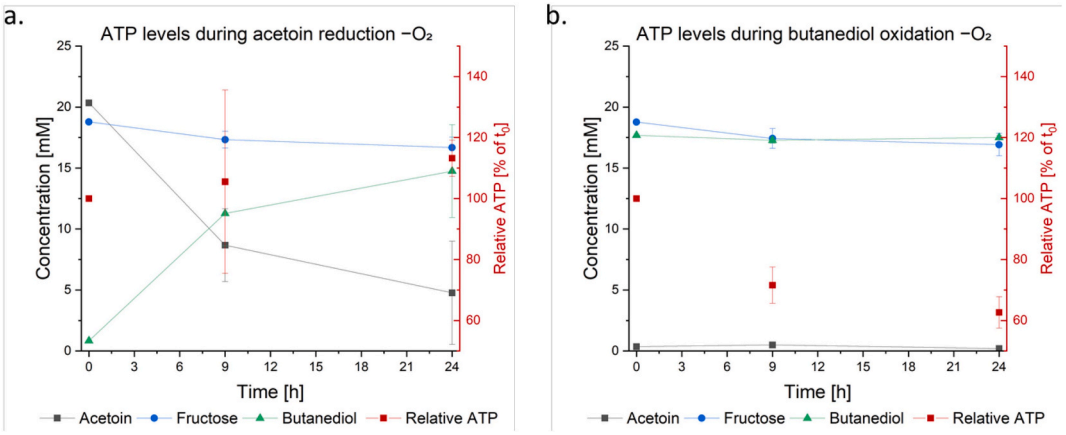

Fig. 6. Relative intracellular ATP levels during anoxic acetoin reduction and 2,3-butanediol oxidation. Cell suspension assays were performed under anoxic conditions with the acetoin-producing strain supplemented with either (a) 20 mM acetoin and 20 mM fructose or (b) 20 mM 2,3-butanediol and 20 mM fructose. Acetoin, 2,3-butanediol, and fructose concentrations are shown on the left y-axis, while relative intracellular ATP levels, normalized to OD_{600} and expressed relative to the initial value ($t_0 = 100\%$), are shown on the right y-axis.

cycle releases up to 24 electrons per fructose molecule. In the here presented experiments, the consumption of approximately 18.6 mM fructose translates theoretically to around 446 mM total electrons generated. However, only about 18 mM electrons, corresponding to a maximum of approximately 9 mM acetoin reduced to 2,3-butanediol, were recovered in the product. This demonstrates that acetoin reduction accounts for merely ~4% of the total electron flux, with the vast majority shunted through the respiratory chain to oxygen to maximize ATP synthesis.

In contrast, strains engineered to express *alsSD* along with *budC* preferentially direct electrons towards acetoin and ultimately to 2,3-BDO, despite abundant oxygen availability (Weiler et al. 2024). The strong promoter driving *alsS* and *alsD* expression apparently creates a high-capacity biosynthetic branch that kinetically outcompetes native respiratory processes for pyruvate and NADH. Specifically, AlsS catalyzes the condensation of two pyruvate molecules into acetolactate and CO_2, followed by AlsD decarboxylating acetolactate into acetoin and CO_2. This leads to fast in-situ acetoin production, which BudC rapidly reduces. Such an efficient pathway diverts 60–90% of carbon flux towards 2,3-BDO, even at transiently low acetoin concentrations (Weiler et al. 2024).

Despite the prevalence of oxygen, the persistence of acetoin reduction underscores its functional role beyond mere energetics. By converting acetoin to 2,3-BDO, *C. necator* oxidizes NADH to NAD^+, sustaining glycolytic flux—particularly when respiratory capacity is transiently limited. This phenomenon parallels overflow metabolism observed in *E. coli*, where acetate is excreted aerobically under nutrient-rich conditions to preserve redox balance and prevent cofactor imbalances (Millard et al. 2021; el-Mansi und Holms 1989). In overflow metabolism, despite the abundance of oxygen, the respiratory capacity seems to be insufficient to keep pace with the rapid NADH generation from glycolysis, necessitating alternative pathways to maintain cellular homeostasis. Products like acetate (or here, 2,3-BDO) thus serve not only to regenerate NAD^+ but also to avoid intracellular acidification under oxic, high-flux conditions.

4.2. Oxygen-Dependent acetoin reduction dynamics

The cell suspension assays reveal oxygen-dependent metabolic priorities in *C. necator* biotransformations, extending observations from engineered strains (Weiler et al. 2024). Under anoxic conditions, overexpressed *budC* catalyzes near-complete acetoin conversion to 2,3-BDO—consuming 20.1 mM acetoin to produce 18.8 mM 2,3-BDO (93% molar efficiency)—despite minimal fructose utilization of only 4.8 mM at 0.2 $mM \cdot h^{-1}$. This reflects acetoin serving as the primary terminal electron acceptor via overexpressed *budC*, reoxidising NADH to NAD^+, while fructose catabolism via the Entner-Doudoroff pathway and hydrogen oxidation together supply the reducing equivalents (see the electron balance below). Minor acetate accumulation (≤2 mM after 24 h) reflects the limited disposal of acetyl-CoA under these conditions rather than a significant electron sink. Under anoxia the tricarboxylic acid cycle cannot turn over without a terminal electron acceptor, and no tricarboxylic-acid-cycle intermediates accumulated, indicating that fructose oxidation stops at the pyruvate dehydrogenase reaction. Entner-Doudoroff catabolism yields one NADH and one NADPH per hexose (the latter usable via transhydrogenase), while pyruvate dehydrogenase flux is capped by acetyl-CoA disposal, as the strain lacks poly(3-hydroxybutyrate) synthase and only ~2 mM acetate accumulated. The resulting reducing equivalents (~11 mM) thus account for much, but not all, of the ~18 mM 2,3-BDO formed, and the peak rate (1.9 mM h^{-1}) exceeds the concurrent fructose uptake (0.26 mM h^{-1}); the remainder is most plausibly supplied by hydrogen oxidation through the NAD^+-reducing soluble hydrogenase. Headspace micro-gas chromatography resolved no net hydrogen consumption, but the turnover required (~1–2% of the headspace pool) lies below its resolution, so a hydrogen contribution is likely but can be neither confirmed nor excluded. We note that soluble hydrogenase activity has not been independently measured in the ΔHoxKGM background used here; its contribution to the electron balance is therefore inferred from the residual reducing-equivalent deficit rather than demonstrated directly.

Oxic conditions contrast sharply with anoxic behavior. Fructose depletes rapidly, with 21.6 mM consumed at 2.3 $mM \cdot h^{-1}$, driving transient 2,3-BDO accumulation that peaks at 15.7 mM after 9 h before reversing to acetoin at 0.7 $mM \cdot h^{-1}$, yielding only 2.6 mM final product. This behavior is consistent with previous studies demonstrating that dissolved oxygen availability directly controls the directionality of the acetoin / 2,3–BDO redox couple, with low oxygen levels favoring reduction to 2,3-BDO and oxic conditions promoting re-oxidation to acetoin (Suttikul et al. 2023).

The pronounced reversibility highlights the dominance of respiration over heterologous electron sinks and highlights oxygen as the key determinant directing NADH either toward product formation or respiratory energy generation. These observations are consistent with established microbial redox balancing principles, where neutral fermentation products like 2,3-BDO regenerate NAD^+ to sustain metabolism under anaerobiosis, as demonstrated across Enterobacteriaceae and engineered systems (Yang et al. 2014; Sheng et al. 2023).

4.3. Extending respiratory modulation to 1,3-Propanediol production

To demonstrate *C. necator*'s capacity for oxygen-tunable reductive biotransformations beyond 2,3–BDO the respiratory modulation concept was extended to 1,3-PDO biosynthesis from glycerol. Under anoxic conditions, slow but tightly coupled conversion prevailed over 98 h: 2.4 mM fructose was consumed (from 16.3 mM) while 6.6 mM 1,3-PDO was formed, corresponding to 13.2 mmol electrons fixed (one NADH consumed per 1,3-PDO; 6.6 mM × 2 electrons). Here, the reduction of the glycerol–derived intermediate 3-hydroxypropionaldehyde to 1,3-PDO is the primary electron sink (3-hydroxypropionaldehyde + NADH → 1,3-propanediol + NAD^+), with fructose catabolism via the ED-pathway and hydrogen oxidation supplying the reducing equivalents. Conversely, oxic conditions decoupled flux from productivity: rapid fructose depletion (19.1 mM within 24 h) and sustained glycerol uptake (13.9 mM over 76 h from 39.9 mM initial) produced no detectable 1,3–PDO. The glycerol-to-1,3-propanediol intermediate 3–hydroxypropionaldehyde is efficiently oxidized to 3–hydroxypropionate by native aldehyde dehydrogenase *gabD4*, diverting flux from the reductive sink—as demonstrated by heterologous expression of *C. necator gabD4* in *E. coli* (Chu et al. 2015).

Salinas *et al.* further elucidated 3-HP catabolism in *C. necator*, identifying *mmsA*1-*A*3 as essential for complete assimilation. Their *ΔmmsA*1-*A*3 mutant accumulated 3-HP as an end product, suggesting that blocking downstream metabolism in this study's strain background could trap 3-HPA as 3-HP, potentially enhancing 1,3-PDO titers by reducing oxidative loss of the toxic intermediate (Chu et al. 2015; Salinas et al. 2022).

These results identify oxygen as a flux-control lever that suppresses futile catabolism while increasing the concentrations of reduced metabolites. This is consistent with metabolic engineering precedents in *E. coli*, in which anaerobic shifts increase the formation of 1,3-propanediol approximately threefold through cofactor engineering (Yang et al. 2018). The parallels between the acetoin and glycerol systems suggest a generalizable principle: respiratory modulation may improve evolutionary stability by reducing growth–product tradeoffs while the titers reported here remain at proof–of–concept level. Further optimization, for example fed-batch anoxic phases with transient oxygenation, may enable scalable production of reduced chemicals from renewable substrates such as glycerol.

4.4. Long-term viability under respiratory constraints

The long-term cell suspension assays demonstrate *C. necator*'s remarkable resilience across respiratory regimes, with oxic conditions fostering transient growth and sustained viability (>88% live cells over 744 h), while anoxic setups reveal stability followed by gradual decline (26% viability at endpoint) and aggregate formation. *C. necator*'s obligate respiratory metabolism requires electron transport chain-coupled ATP generation; acetoin reduction via *budC* rebalances NADH/NAD^+ but yields only substrate-level phosphorylation (~1 ATP/fructose vs ~24 ATP via O_2 respiration), causing energetic attrition over weeks (Pearcy et al. 2022). This mirrors denitrification studies where fructose + NO_3^- sustains anoxia via proton motive force, but acetoin alone fails despite redox handling. Cell aggregation post-48 h may reflect ATP-limited stress responses.

These dynamics parallel *C. necator* H16 models under oxygen-limited autotrophy, where O_2 restriction boosts PHB via respiratory down-regulation (e.g., 310% higher yields despite 30% growth penalty) and viability attrition reflects curtailed ATP from substrate-level phosphorylation alone (Tang et al. 2020).

4.5. ATP maintenance during anoxic acetoin reduction

ATP measurements performed under anoxic conditions further support the hypothesis that the reduced cell viability observed during oxygen starvation is attributable to insufficient ATP availability. Continuous acetoin reduction maintained intracellular ATP levels over 24 h, whereas ATP levels declined markedly in cultures supplemented with 2,3-butanediol. This indicates that acetoin reduction contributes to cellular energy conservation under respiratory constraints and supports the concept that oxygen limitation can couple productive biotransformation to cellular fitness. Consequently, coupling ATP maintenance to productive acetoin reduction may reduce the selective advantage of non-producing variants and thus represents a promising basis for the development of cellular addiction systems in future metabolic engineering approaches.

The implementation of such strategies under defined hydrogen/nitrogen atmospheres rather than air does, however, impose practical constraints. Handling hydrogen–containing gas mixtures requires dedicated safety measures, maintaining oxygen-free conditions increases process complexity, and the low aqueous solubility of hydrogen may become a mass-transfer limitation at industrial scale. These challenges must be balanced against the benefits of respiratory control, and future process concepts combining controlled anoxic production phases with optimized gas transfer may help to overcome these limitations.

5. Conclusion

This study demonstrates that oxygen availability functions as a control parameter for intracellular redox metabolism in *Cupriavidus necator*. By modulating the availability of the terminal electron acceptor, metabolic flux can be directed either toward reductive product formation or toward respiratory energy generation. Under anoxic conditions and a hydrogen-containing atmosphere, the reduction of acetoin to 2,3-butanediol and of glycerol to 1,3-propanediol acts as an effective electron sink, with hydrogen oxidation via the soluble hydrogenase supplying the reducing equivalents in the absence of respiration. In contrast, oxic conditions favor re-oxidation through the electron transport chain, leading to product re-oxidation and enhanced cell maintenance. These findings establish oxygen as a key lever for decoupling growth from product formation and provide a foundation for dynamic process-control strategies aimed at improving the productivity and process robustness of engineered microbial biotransformations.

CRediT authorship contribution statement

Vivien Jesenofsky: Writing – original draft, Visualization, Investigation, Data curation, Conceptualization. **Janek R. Weiler:** Writing – original draft, Visualization, Methodology, Conceptualization. **Johannes Gescher:** Writing – review & editing, Supervision, Resources, Project administration, Funding acquisition, Conceptualization. **Miriam Edel:** Writing – review & editing, Writing – original draft, Supervision, Project administration, Conceptualization.

Declaration of competing interest

The authors declare that they have no known competing financial interests or personal relationships that could have appeared to influence the work reported in this paper.

Acknowledgements

This project is funded by the Deutsche Forschungsgemeinschaft (DFG, German Research Foundation) – SFB 1615 – 503850735. The graphical abstract was created in BioRender. Edel, M. (2026) https://BioRender.com/lc25qsc.

Appendix A. Supplementary data

Supplementary data to this article can be found online at https://doi.org/10.1016/j.biortech.2026.135473.

Data availability

All data collected and reported in this study have been made available under copyright at TUHH Open Research (TORE): https://doi.org/10.15480/882.16935.

References

Alagesan, S., Hanko, E.K.R., Malys, N., Ehsaan, M., Winzer, K., Minton, N.P., 2018. Functional genetic elements for controlling gene expression in *Cupriavidus necator H16*. Appl. Environ. Microbiol. 84, e00878–e00918. https://doi.org/10.1128/AEM.00878-18.

Becker, L., Dietz, E., Holtmann, D., 2025. Individual process steps optimization of *Cupriavidus necator*-catalyzed production of α-humulene. Biochem. Eng. J. 215. https://doi.org/10.1016/j.bej.2024.109617. S. 109617.

Chu, Hun Su; Kim, Young Soo; Lee, Chan Mu; Lee, Ju Hee; Jung, Won Seok; Ahn, Jin-Ho et al. (2015): Metabolic engineering of 3-hydroxypropionic acid biosynthesis in *Escherichia coli*. In: *Biotechnology and bioengineering* 112 (2), S. 356–364. DOI: 10.1002/bit.25444.

el-Mansi, E. M.; Holms, W. H. (1989): Control of carbon flux to acetate excretion during growth of *Escherichia coli* in batch and continuous cultures. In: *Journal of general microbiology* 135 (11), S. 2875–2883. DOI: 10.1099/00221287-135-11-2875.

Enfors, S.O., Jahic, M., Rozkov, A., Xu, B., Hecker, M., Jürgen, B., et al., 2001. Physiological responses to mixing in large scale bioreactors. J. Biotechnol. 85 (2), 175–185. https://doi.org/10.1016/s0168-1656(00)00365-5.

Gibson, D., Young, L., Chuang, R.Y., Venter, J.C., Hutchison, C.A., Smith, H.O., 2009. (2009) Enzymatic assembly of DNA molecules up to several hundred kilobases. Nat. Methods 6, 343–345. https://doi.org/10.1038/nmeth.1318.

Härrer, Daniel; Windhorst, Carina; Böhner, Nicola; Novion Ducassou, Julia; Couté, Yohann; Gescher, Johannes (2021): Production of acetoin from renewable resources under heterotrophic and mixotrophic conditions. In: *Bioresource technology* 329, S. 124866. DOI: 10.1016/j.biortech.2021.124866.

Karcagi, Ildikó; Draskovits, Gábor; Umenhoffer, Kinga; Fekete, Gergely; Kovács, Károly; Méhi, Orsolya et al. (2016): Indispensability of Horizontally Transferred Genes and Its Impact on Bacterial Genome Streamlining. In: *Molecular biology and evolution* 33 (5), S. 1257–1269. DOI: 10.1093/molbev/msw009.

Lara, Alvaro R.; Galindo, Enrique; Ramírez, Octavio T.; Palomares, Laura A. (2006): Living with heterogeneities in bioreactors: understanding the effects of environmental gradients on cells. In: *Molecular biotechnology* 34 (3), S. 355–381. DOI: 10.1385/MB:34:3:355.

Li, Han; Opgenorth, Paul H.; Wernick, David G.; Rogers, Steve; Wu, Tung-Yun; Higashide, Wendy et al. (2012): Integrated electromicrobial conversion of CO2 to higher alcohols. In: *Science (New York, N.Y.)* 335 (6076), S. 1596. DOI: 10.1126/science.1217643.

Millard, Pierre; Enjalbert, Brice; Uttenweiler-Joseph, Sandrine; Portais, Jean-Charles; Létisse, Fabien (2021): Control and regulation of acetate overflow in *Escherichia coli*. In: *eLife* 10. DOI: 10.7554/eLife.63661.

Neubauer, Peter; Junne, Stefan (2010): Scale-down simulators for metabolic analysis of large-scale bioprocesses. In: *Current opinion in biotechnology* 21 (1), S. 114–121. DOI: 10.1016/j.copbio.2010.02.001.

Pearcy, N., Garavaglia, M., Millat, T., Gilbert, J.P., Song, Y., Hartman, H., et al., 2022. A genome-scale metabolic model of *Cupriavidus necator* H16 integrated with TraDIS and transcriptomic data reveals metabolic insights for biotechnological applications. PLoS Comput. Biol. 18 (5), e1010106. https://doi.org/10.1371/journal.pcbi.1010106.

Pohlmann, Anne; Fricke, Wolfgang Florian; Reinecke, Frank; Kusian, Bernhard; Liesegang, Heiko; Cramm, Rainer et al. (2006): Genome sequence of the bioplastic-producing "Knallgas" bacterium *Ralstonia eutropha* H16. In: *Nat Biotechnol* 24 (10), S. 1257–1262. DOI: 10.1038/nbt1244.

Rugbjerg, Peter; Sarup-Lytzen, Kira; Nagy, Mariann; Sommer, Morten Otto Alexander (2018): Synthetic addiction extends the productive life time of engineered *Escherichia coli* populations. In: *Proceedings of the National Academy of Sciences of the United States of America* 115 (10), S. 2347–2352. DOI: 10.1073/pnas.1718622115.

Rugbjerg, P., Sommer, M.O.A., 2019. Overcoming genetic heterogeneity in industrial fermentations. Nat. Biotechnol. 37 (8), 869–876. https://doi.org/10.1038/s41587-019-0171-6.

Salinas, Alejandro; McGregor, Callum; Irorere, Victor; Arenas-López, Christian; Bommareddy, Rajesh Reddy; Winzer, Klaus et al. (2022): Metabolic engineering of *Cupriavidus necator* H16 for heterotrophic and autotrophic production of 3-hydroxypropionic acid. In: *Metabolic engineering* 74, S. 178–190. DOI: 10.1016/j.ymben.2022.10.014.

Sheng, Lili; Madika, Abubakar; Lau, Matthew S. H.; Zhang, Ying; Minton, Nigel P. (2023): Metabolic engineering for the production of acetoin and 2,3-butanediol at elevated temperature in *Parageobacillus thermoglucosidasius* NCIMB 11955. In: *Frontiers in bioengineering and biotechnology* 11, S. 1191079. DOI: 10.3389/fbioe.2023.1191079.

Suttikul, S., Charalampopoulos, D., Chatzifragkou, A., 2023. Biotechnological production of Optically Pure 2,3-butanediol by *Bacillus subtilis* based on dissolved oxygen control strategy. In: Fermentation 9 (1), S. 15. https://doi.org/10.3390/fermentation9010015.

Sydow, Anne; Krieg, Thomas; Ulber, Roland; Holtmann, Dirk (2017): Growth medium and electrolyte-How to combine the different requirements on the reaction solution in bioelectrochemical systems using *Cupriavidus necator*. In: *Engineering in life sciences* 17 (7), S. 781–791. DOI: 10.1002/elsc.201600252.

Tang, R., Weng, C., Peng, X., Han, Y., 2020. Metabolic engineering of *Cupriavidus necator* H16 for improved chemoautotrophic growth and PHB production under oxygen-limiting conditions. Metab. Eng. 61, 11–23. https://doi.org/10.1016/j.ymben.2020.04.009.

Vandecraen, Joachim; Chandler, Michael; Aertsen, Abram; van Houdt, Rob (2017): The impact of insertion sequences on bacterial genome plasticity and adaptability. In: *Critical reviews in microbiology* 43 (6), S. 709–730. DOI: 10.1080/1040841X.2017.1303661.

Weiler, Janek R.; Jürgensen, Nikolai; Cornejo Infante, Monica; Knoll, Melanie T.; Gescher, Johannes (2024): Strain and model development for auto- and heterotrophic 2,3-butanediol production using *Cupriavidus necator* H16. In: *Biotechnology for biofuels and bioproducts* 17 (1), S. 108. DOI: 10.1186/s13068-024-02549-7.

Windhorst, C., Gescher, J., 2019. Efficient biochemical production of acetoin from carbon dioxide using *Cupriavidus necator* H16. In: Biotechnol. Biofuels 12. https://doi.org/10.1186/s13068-019-1512-x. S. 163.

Yang, B., Liang, S., Liu, H., Liu, J., Cui, Z., Wen, J., 2018. Metabolic engineering of *Escherichia coli* for 1,3-propanediol biosynthesis from glycerol. Bioresour. Technol. 267, 599–607. https://doi.org/10.1016/j.biortech.2018.07.082.

Yang, Taek Ho; Rathnasingh, Chelladurai; Lee, Hee Jong; Seung, Doyoung (2014): Identification of acetoin reductases involved in 2,3-butanediol pathway in *Klebsiella oxytoca*. In: *Journal of biotechnology* 172, S. 59–66. DOI: 10.1016/j.jbiotec.2013.12.007.